PAPER • OPEN ACCESS

Improving Acoustic Methods of Pipeline Leak Location with Distributed Sensing

To cite this article: Joshua Z. Hooper *et al* 2024 *J. Phys.: Conf. Ser.* **2647** 192010

View the article online for updates and enhancements.

Improving Acoustic Methods of Pipeline Leak Location with Distributed Sensing

Joshua Z. Hooper, Michal Kalkowski, and Jennifer M. Muggleton

Institute of Sound and Vibration Research, University of Southampton, Southampton, SO17 1BJ

E-mail: `J.Z.Hooper@soton.ac.uk`

Abstract. Leaks in water distribution mains are a big problem, with around 20% of supplied potable water lost to leaks during transport. Correlation-based acoustic techniques have provided an accurate and non-invasive way of detecting and locating these leaks for a few decades. These methods have almost exclusively been using two sensors, and so this paper presents work aiming to explore leak detection and location with multiple sensors distributed along a pipe. Beamforming is a well-established method for using arrays of sensors to locate sources, among other purposes. With this premise, the present work adopts an array processing algorithm (MUSIC) in the context of water leak detection, intending to develop a framework for detecting multiple leaks using a sensor array. The concept, processing and implementation details are first supported with numerical simulations using existing acoustic models of water pipes. Then, experiments are presented on a short section of water-filled pipe with leak-like disturbances. These are captured with an array of accelerometers and processed using an implementation of the algorithm, testing the impact of real-world effects studied in simulations. The study considers several aspects of practical interest: (i) the effect of noise, both correlated and uncorrelated; (ii) the effect of reflections from discontinuities, such as pipe fittings and connections; (iii) the number and the distribution of sensors; as well as (iv) the presence of multiple leaks. The results pave the way for implementing this algorithm on practical installation designs, including the rod method developed during a wider research project associated with this study.

1. Introduction
Leaks are a major problem in water distribution systems across the world, with recent estimates suggesting that billions of litres of water are lost to leakage in the UK alone - around 20% of the supply. The ecological and economic impacts of this are major, and potable water supply security in the coming years is a growing concern for many countries. Effective methods of detecting and finding these leaks are therefore a vital task. Many methods of leak detection already exist [1], of which acoustic methods are often preferred due to their non-invasive nature and potential accuracy. Central to the functioning of acoustic methods of leak detection is the fact that a burst in the pipe, or a loose fitting along it, produces an acoustic signal in the form of noise; this is of significant amplitude when the water is under enough pressure. This noise can be characterised, and therefore picked up at sensors along the pipe to be analysed.

What has become the standard approach to acoustic leak detection is called the cross-correlation method. Cross-correlation is a statistical signal processing tool used to evaluate the similarity of two signals according to the relative delay between them. Computing this

should reveal a difference in the propagation time from a common noise source between, as in the case of leak location, two sensors. When the distance between two sensors is known, the location of the source can be estimated with the relative time delay and the wavespeed in the pipe, according to the fact that a planar acoustic wave travelling a distance d with speed c will take time $t = d/c$. A more full outline of this method, as well as a review of its effectiveness in a live practical implementation, is given in Ref. [2]. Although this method has proven effective, there are a few shortcomings. Firstly, it is naturally a more manual approach, in that two sensor locations have to be chosen based on the suspicion of a leak in a general area. Second, there is a difficulty when more than one leak is present between two sensors, causing extra peaks in the cross-correlation, which are harder to analyse. There is also a reliance upon an accurate value of the wavespeed, which means the method is dependent either upon an accurate model of the system, or an effective means of determining the wavespeed experimentally.

With the proliferation of cheaper and more advanced electronic sensing and better communication between those sensors, it seems natural to consider the extension of acoustic leak detection to more than the two sensors used in conventional cross-correlation. Large sensor networks are often referred to as distributed sensing systems, and can offer increased accuracy and resolution - it is the hope of the present research that such a system will alleviate some of the aforementioned issues with the cross-correlation method. This paper first details an algorithm which can detect multiple sources over an array of sensors (Section 2) and examines the applicability of this to the leak location problem. Then, results of this algorithm as applied to simulated and experimental data (Sections 4 and 5) of a pipe leak scenario are presented, with the acoustic model used to produce these results briefly outlined in Section 3.

2. Leak location using distributed sensing

Localising the source of a signal from an array of sensors is a common and well-understood problem within signal processing and acoustics, with beamforming being a classic example of an approach successfully applied to a variety of problems [3]. Therefore we have drawn upon similar array processing techniques when looking at the specific topic of leak detection.

2.1. Source location using Multiple Signal Classification

This research employs a subspace-based array processing algorithm called Multiple Signal Classification (MUSIC), originally developed by Schmidt [4], which determines the number of sources present and where they have come from. MUSIC has seen interest in a variety of domains, such as radar, sonar, seismology, and non-destructive evaluation (NDE), from which the notation in this paper has been adapted.

The set-up for this method is to determine the vectors of the source signals by estimating the points of origin from collected data. Signals are collected at N sensors, from which the covariance matrix $\mathbf{C}$ is computed. The core of the algorithm is in the singular value decomposition (SVD) of this covariance matrix. For M present signal sources, there will be M significant singular values in the ideal case, with the other $N - M$ being zero (or below a determined negligible level in the non-ideal case). Because of this, a separation can be made between the signal subspace and the noise subspace in the corresponding eigenvectors. Then, these vectors can be compared to an assumed ideal response of the system under study, according to the orthogonality of the subspaces [4].

As mentioned, the field of non-destructive evaluation (NDE) has made use of subspace methods in imaging. For instance, time-reversal imaging uses singular value decomposition to extract dominant components of the signal, and synthetically back-propagate them to candidate source locations, producing a wave-based image. The time reversal operator used in the active case (with the array both transmitting and receiving) is analogous to the covariance matrix captured using a receiver-only array [5, 6]. While time-reversal imaging and MUSIC are

somewhat related, the former is formulated in the frequency domain, allowing for wideband signals to be analysed - necessary when considering the case of leak noise. Classical MUSIC, on the other hand, was developed for narrowband signals, which results in a single $N \times N$ covariance matrix.

Signals are collected at N sensors in an array, for a number of observations P. The signal, $x_{ij}(t)$, at sensor $i \in [0, N]$ for acquisition $j \in [0, P]$ is put into an acquisition matrix A (in the frequency domain),

$$\mathbf{A}(\omega) = \begin{pmatrix} X_{11}(\omega) \cdots\cdots\cdots X_{1P}(\omega) \\ \vdots \quad \ddots \quad\quad\quad \vdots \\ X_{N1}(\omega) \cdots\cdots\cdots X_{NP}(\omega) \end{pmatrix}, \tag{1}$$

where $X_{ij}(\omega) = \mathbb{F}\{x_{ij}(t)\}$ is the Fourier transform of the time series at each sensor. Then the frequency-domain covariance matrix,

$$\mathbf{C}(\omega) = \mathbf{A}(\omega)\mathbf{A}(\omega)^H, \tag{2}$$

is computed for the set of signal observations. The superscript H is the conjugate transpose (Hermitian) operation.

To retrieve the signal and noise vectors and singular values, a singular value decomposition is applied to the covariance matrix,

$$\mathbf{C} = \mathbf{U}\boldsymbol{\Sigma}\mathbf{V}^H, \tag{3}$$

where $\mathbf{U}$, $\mathbf{V}^H$ are $N \times N$ matrices whose columns (rows) are the left (right)-singular vectors of $\mathbf{C}$, and $\boldsymbol{\Sigma}$ is a diagonal matrix of the singular values σ_i of $\mathbf{C}$. $\mathbf{U}$ and $\mathbf{V}^H$ are unitary matrices, and the singular vectors which make them up form orthonormal bases.

The singular vectors $\mathbf{U}$ can now be separated into the signal and noise subspaces, $\mathbf{U}_s, \mathbf{U}_n$, for processing; $\mathbf{U}_s$ is composed of the M significant singular vectors, and $\mathbf{U}_n$ of the other $N - M$ vectors. The vectors of the signal subspace should be estimates of the contribution from a given source to the signals recorded at each of the N sensors.

Now, the locations of sources are found by comparison of the singular vectors, $\mathbf{U}_n$ or $\mathbf{U}_s$, with the vectors of the ideal sensor responses $\mathbf{g}(r)$ for a source at a postulated location r. In this context, the ideal response will be composed of the Green's functions of the system computed at a given frequency ω, from a source at the test position r to each of the sensor positions r_i:

$$\mathbf{g}(r) = [G(r_1, r, \omega), ..., G(r_N, r, \omega)], \tag{4}$$

where

$$G(r_i, r, \omega) = \mathrm{e}^{-ik(\omega)\|r-r_i\|}. \tag{5}$$

A (normalised) single frequency ω image is calculated from a 'central frequency' operator [7],

$$A(r, \omega) = \frac{\mathbf{g}^H(r,\omega)\mathbf{U}_n \cdot \mathbf{U}_n^H \mathbf{g}(r,\omega)}{\|\mathbf{g}(r,\omega)\|^2} = 1 - \frac{\mathbf{g}^H(r,\omega)\mathbf{U}_s \cdot \mathbf{U}_s^H \mathbf{g}(r,\omega)}{\|\mathbf{g}(r,\omega)\|^2}, \tag{6}$$

which should return a value approaching unity when the test position coincides with a signal source, and should vanish away from these points in the ideal case, due to the orthogonality of the signal and noise subspaces. The peaks of the operator $A(r, \omega)$ can then be read off as the location estimates of the present leaks. This information can also be displayed as an image, as is done in Section 4. A multi-frequency form (this is often what is referred to as TR-MUSIC in the acoustic imaging community [7]) provides more robustness and a clearer image. This is achieved by summing the contribution of the operator $A(r, \omega)$ at each frequency and normalising

by dividing by the number of frequency bins so that the image $I(r, \Omega)$ over a range of frequencies Ω is

$$I(r, \Omega) = \frac{1}{\frac{1}{N_\omega} \sum_i^{N_\omega} A(r, \omega_i)}, \tag{7}$$

where N_ω is the number of frequency bins used in Ω. Either the noise or signal subspace can be used, with the choice determined by the expected number of sources and the signal-to-noise ratio (SNR) of a given scenario.

The efficacy of this imaging function will be studied in Section 4, as well as a comparison of the effect of using the signal subspace versus the noise subspace in the computation.

3. Modelling of leak noise propagation

Since the MUSIC algorithm requires an assumed (theoretical) response at each point in space, an accurate acoustic model is necessary. Thankfully, much work has already been done to develop and refine analytical modelling of wave propagation in water pipes [8, 9, 10, 11], because the cross-correlation method requires an accurate wavespeed estimate. This work included characterisation of the propagation in different pipe wall materials, from which the insights gained will be indispensable in the real-world implementation of MUSIC-based source location. The acoustic model presented here will also be used to run numerical simulations shown in subsequent sections.

3.1. Free wave propagation

Pinnington and Briscoe [11] developed a model of acoustic wave propagation in pipes, building on previous work [9], deriving wavenumber expressions from equations of motion which are simplified forms of Kennard's equations for different modes of vibration. The equations of motions used are expressed in terms of n *circumferential modes*, each of which has s "branches" of dispersion cutting in at different frequencies. In practice, the pipe leaks predominantly excite the fluid-borne radially axisymmetric wave ($n = 0$, $s = 1$), for which the derived expression is

$$k_1^2 = k_f^2 \left(1 + \frac{2B_f/a}{E_p h/a^2 - \omega^2 \rho_p h} \right), \tag{8}$$

where k_f is the wavenumber of the fluid; B_f is the bulk modulus of the fluid, E_p is the Young's modulus of the shell (pipe), h is the radius of the shell, a is the thickness of the shell wall, ρ_p is the density of the shell, and ω is the (angular) frequency. The form of Eqns. 8 are as expressed by Muggleton et al. [8] as compared to the non-dimensionalised form seen in Ref. [11]. Although the fluid-borne wave is dominant, consideration of the different wavenumbers and different modes may in the future aid in improving the accuracy of a system, so that they are well-suited for practical sensor setups.

Supplied with a wavenumber expression, wave propagation in an infinite pipe can be modelled in the frequency domain as

$$X_i(\omega) = H(\omega, |r_i - r_{leak}|) X_{leak}(\omega), \tag{9}$$

where $H(\omega, r) = e^{ik(\omega)r}$ is the transfer function between the leak and the sensor, and r_i, r_{leak} are the positions of the sensor and leak, respectively.

3.2. Steady-state response of a finite pipe

In order to take into account practical effects such as reflections, we consider the case of a finite pipe, where the ends are characterised by reflection coefficients R_i at $x = 0$, $x = L$, as illustrated in Fig. 1. Following the propagation of waves for a single mode across characteristic locations
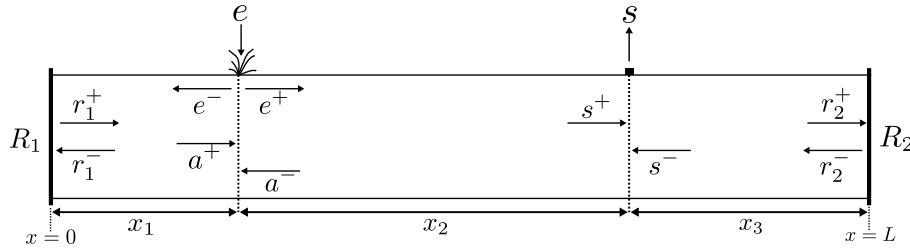
Figure 1: Diagram of the propagation of a single acoustic wave mode when considering reflections in the pipe, for a leak at position x_1, reading at a sensor at position $x_1 + x_2$.

in both directions, we can write the following series of equations for the steady-state harmonic motion:

$$
\begin{aligned}
s^+ &= a^+ e^{-ikx_2}, & a^+ &= e^+ + r_1^+ e^{-ikx_1}, & r_1^+ &= R_1 r_1^-, \\
r_1^- &= a^- e^{-ikx_1}, & a^- &= s^- e^{-ikx_2} + e^-, & s^- &= r_2^- e^{-ikx_3}, \\
r_2^- &= R_2 r_2^+, & r_2^+ &= s^+ e^{-ikx_3}.
\end{aligned}
\tag{10}
$$

Using these to calculate the response $s(\omega) = s^+(\omega) + s^-(\omega)$ observed by a sensor at a point $x = x_1 + x_2$ on the pipe,

$$
s = \frac{e^+ e^{-ikx_2} + e^- R_1 e^{-2ikx_1} e^{-ikx_2}}{1 - R_1 R_2 e^{-2ikL}} (1 + R_2 e^{-2ikx_3}),
\tag{11}
$$

where e^+, e^- are the positive- and negative-going pressure waves emitted by the leak at position x_1; x_2 is the distance between the leak and the sensor; x_3 is the distance between the sensor and the right-hand boundary at $x = L$; $k = k(\omega)$ is the wavenumber (Eqn. 8) at a given frequency ω. This expression will be used in numerical simulations of the leak detection scenario when simulating shorter, finite pipes. In the case of an infinite pipe, $R_1 = R_2 = 0$, for which Eqn. 11 simply reduces to the simple transfer function expression of Eqn. 9.

4. Simulated results
Using the analytical model discussed in Section 3, a numerical simulation has been set up to give a basic proof of concept for applying the TR-MUSIC algorithm to leak signals in a water pipe. For the following figures, a pipe of length $L = 200\,\text{m}$ has been chosen, made of high-density polyethylene (HDPE) with material properties listed in Table 1. The model represents a leak signal with zero-mean Gaussian white noise, and the response at each sensor location is calculated using the wavenumber expression (Eqn. 8) input into the reflection transfer function (Eqn. 11). These signals are then inverse Fourier-transformed to simulate an acquisition matrix that would in practice come from measurements. Noise can be added to represent different disturbances, such as uncorrelated sensor noise, a correlated source which might come from the surrounding environment, or a tonal source that might be emitted by machinery nearby.

Initially, we consider a simple configuration to show a basic proof of concept - that is, a single leak with no end reflections, and with uniformly spaced sensors. Some uncorrelated noise, with SNR 20 dB w.r.t the source amplitude[1], is added to simulate the case of noise from the sensors or from the environment. Figure 2a shows the output image in this case, with results from

---

[1] This sounds like a low noise level, but because of attenuation in the pipe, the SNR at each sensor is much lower, varying according to the distance from the signal source.

Table 1: Pipe properties, used for simulation and imaging, for a HDPE (high-density polyethylene) pipe.

Pipe property	Value
Young's modulus, E_p	$0.76 \times 10^9 \, \text{Pa}$
Radius, a	$55 \times 10^{-3} \, \text{m}$
Thickness, h	$6.9 \times 10^{-3} \, \text{m}$
Density, ρ_p	$930 \, \text{kg} \, \text{m}^{-3}$
Poisson's ratio, ν_p	0.4
Material loss factor, η	0.056
Plate compressional wavespeed, c_L	$1725 \, \text{m} \, \text{s}^{-1}$

both the noise and signal subspace versions plotted. A clear peak is shown at the leak location, resolved to the image point closest to the input location.

A key reason for the algorithmic approach taken was the ability to resolve the location of multiple leaks present across the array, thus much of the testing presented has been carried out with this as the case. Figure 2b shows the simulated results with the same setup as the single leak, but now with three leaks at $20 \, \text{m}$, $104 \, \text{m}$ and $167.2 \, \text{m}$. It can be seen that each individual leak is resolved well, standing clearly above the noise of the data.

The separate results shown for the signal subspace and noise subspace shown in Fig. 2 show that both of these versions work to localise the noise sources, but behave slightly differently. The noise subspace is more affected by the noise in the data, seen in the higher amplitude side lobes and slightly broader peaks. The exact origin of the behaviour of these different subspaces is reserved for future research.
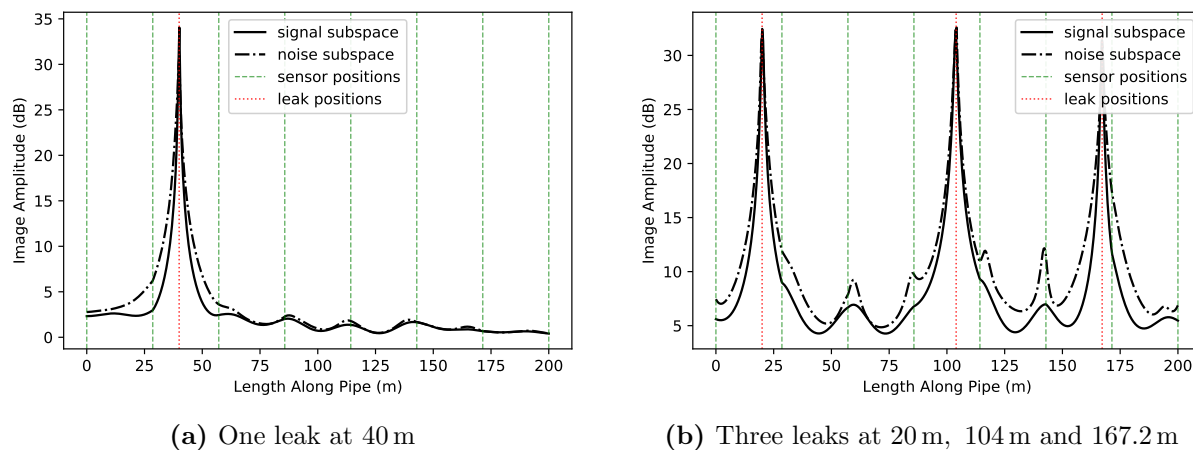

(a) One leak at $40 \, \text{m}$

(b) Three leaks at $20 \, \text{m}$, $104 \, \text{m}$ and $167.2 \, \text{m}$

Figure 2: Images from the TR-MUSIC algorithm scanned from $1 \, \text{Hz}$ to $4 \, \text{Hz}$ with both the signal subspace (——) and noise subspace (— · —) displayed. No reflections are simulated and data is generated with a period of $1 \, \text{s}$ over 16 iterations. Each sensor has SNR of $20 \, \text{dB}$ w.r.t. source.

4.1. Effect of sensor density and frequency range
Now that the effectiveness of the general procedure has been demonstrated, we proceed to show the effect of some of the parameters, in particular the frequencies chosen to form the image, and

the number of sensors in the array. These become clearest when observing the case where two leaks fall close to each other, as is shown in Fig. 3.

Taking the same setup as used for Fig. 2, noise sources are instead situated at $20\,\text{m}$, $160\,\text{m}$, and $167.2\,\text{m}$. Fig. 3a shows the image produced scanning up to $4\,\text{Hz}$, where it can be seen that only two peaks are present, with the two closer noise sources unresolved individually and the peak lying at roughly their midpoint instead. The reason for this is that the frequencies used in the algorithm affect the wavelength of the resulting image due to the use of the Green's function with a particular frequency in the computation. For a given frequency chosen in the algorithm, f_{img}, the wavelength of the resulting image is determined by

$$\lambda = \frac{c}{2f_{\text{img}}}, \tag{12}$$

where c is the effective wavespeed, $c = \omega/k(\omega)$. When this wavelength is longer than the separation of two noise sources, the algorithm is unable to resolve them.

Instead, higher frequencies can be used to produce an image which has sharper peaks and can then resolve two closely spaced sources. Fig. 3b shows the result when frequencies up to $50\,\text{Hz}$ are used, where each of the noise sources are now well-resolved. What can be noticed with the increased frequency range is some aliasing effects, seen as steps in the amplitude at each of the sensor positions. This happens once the wavelength of the image surpasses that of the spacing of the sensors - effectively, we are going beyond the spatial resolution of the array, and so aliasing is present despite the successful resolution of sources above this wavelength.

The interplay of the spatial frequency (the image, affected by the Green's function) and temporal frequency (the section of spectral cross-correlation used) is more complex and will be part of future research. Limited information is found in the literature, due to the focus on narrowband applications previously mentioned. However, the present simulated results at least show these effects qualitatively.
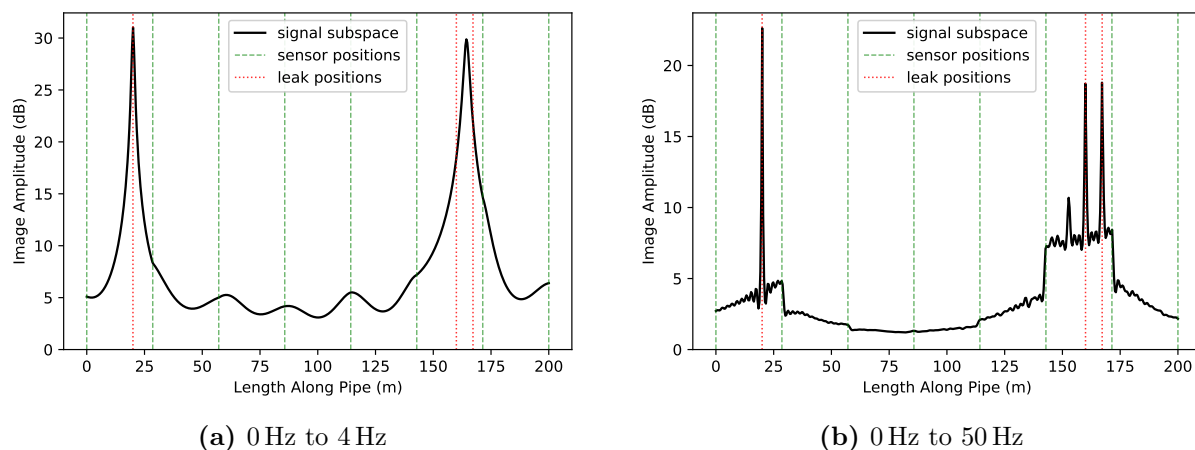

(a) $0\,\text{Hz}$ to $4\,\text{Hz}$ **(b)** $0\,\text{Hz}$ to $50\,\text{Hz}$

Figure 3: Multi-frequency images for the case of multiple noise sources (leaks), showing significant peaks resolved at the chosen leak locations when going above the frequency associated with the sensor spacing. Simulated using a $200\,\text{m}$ pipe with no reflections, and $20\,\text{dB}$ SNR.

Considering the case of different numbers of sensors provides another view on the resolution capability of the algorithm. One might suppose that a larger number of sensors would provide an improved resolution of noise sources due to the extra information, however this is not the case due to the wavelength relationship just described. Fig. 4 shows the result when an array of 32 sensors is used instead of 8. Fig. 4a shows that, for the same lower frequency range as before,

the extra sensors do not improve the resolution. Only when the frequency range is increased (Fig. 4b) can the two close noise sources be resolved. Comparing with this with Fig. 3b, we see that the aliasing effects are less pronounced due to the higher spatial resolution of the array.
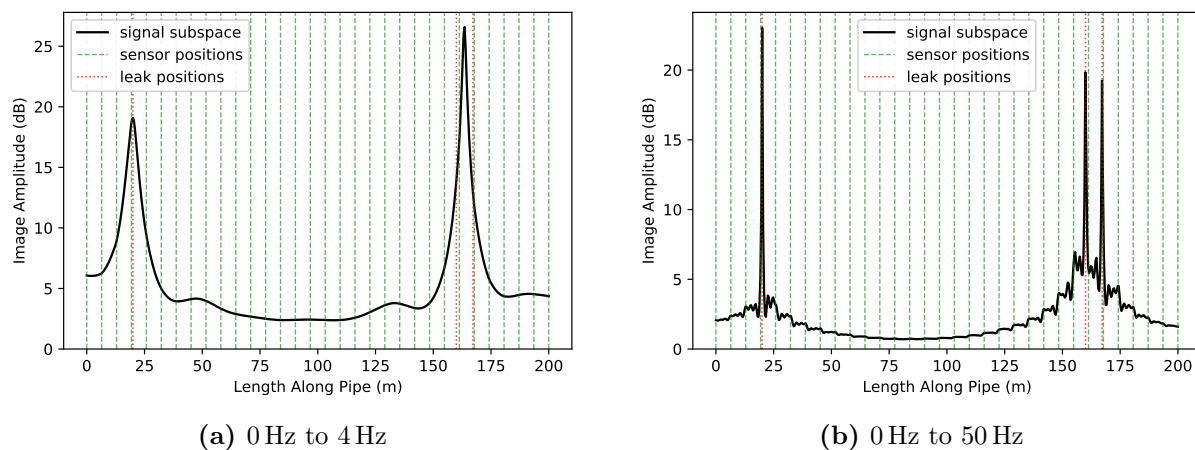

(a) $0\,\mathrm{Hz}$ to $4\,\mathrm{Hz}$

(b) $0\,\mathrm{Hz}$ to $50\,\mathrm{Hz}$

Figure 4: Multi-frequency images for the case of multiple noise sources (leaks), showing significant peaks resolved at the chosen leak locations when going above the frequency associated with the sensor spacing. Simulated using a $200\,\mathrm{m}$ pipe with no reflections, and the presence of additional noise.

4.2. Effect of reflections

Now incorporating the finite pipe model developed in Section 3.2, the effect of reflections on the imaging algorithm is shown in Fig. 5, using the same pipe parameters as before but with a shorter length ($20\,\mathrm{m}$). A spread of reflection coefficients has been used, matching at each end for the sake of simplicity. It can be seen that as the reflection coefficient is increased, there are two main effects - a decrease in the peak image amplitude, and a raised amplitude in the image at the ends. The size of these effects is negligible at small reflection coefficients and then increases as $R_1, R_2 \to 1$.
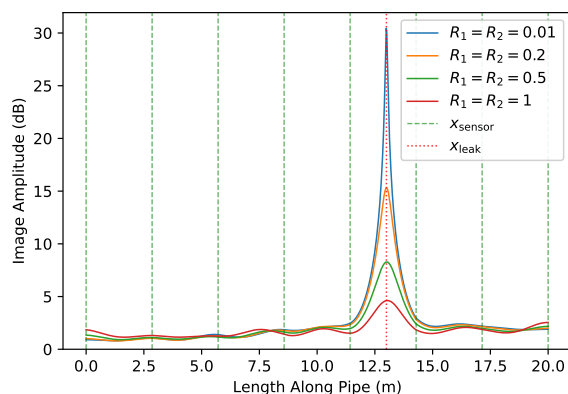

Figure 5: Imaging result for a $20\,\mathrm{m}$ pipe, with varied matching reflection coefficients at both ends. Scanned over frequencies from $0\,\mathrm{Hz}$ to $40\,\mathrm{Hz}$

5. Experimental validation

5.1. Experimental setup

In order to provide a real-world validation of the technique outlined in this paper, a practical pipe rig has been set up to run experiments. A $6\,\mathrm{m}$ length of HDPE pipe has been used - filled with

water (static, and not under pressure), and capped off at each end. The properties of the pipe are given in Table 1, using values given by the manufacturer, except for the Young's modulus, E, and material loss factor, η, which were determined experimentally. Two electrodynamic shakers at different positions along the pipe (2.6 m and 4.8 m) were fed with uncorrelated Gaussian white noise to simulate the noise emitted by two separate leaks. An array of 7 accelerometers, uniformly spaced 0.9 m apart was used to capture the signals, sampling at 8192 Hz for a period of 64 s. These signals were divided into sections of period 1 s, to form an acquisition matrix (Eqn. 1) with 64 iterations (i.e. a 7×64 matrix).

5.2. Results

The multi-frequency imaging algorithm (TR-MUSIC, Eqn. 7) was used to analyse the signals, using a frequency range of 450 Hz to 650 Hz. The resulting image is shown in Fig. 6a, with the result from a simulated set of data shown in Fig. 6b for comparison. Note that the y-axis is no longer on a decibel scale. The background noise level was measured, with the SNR found to be 40 dB w.r.t. the source level.

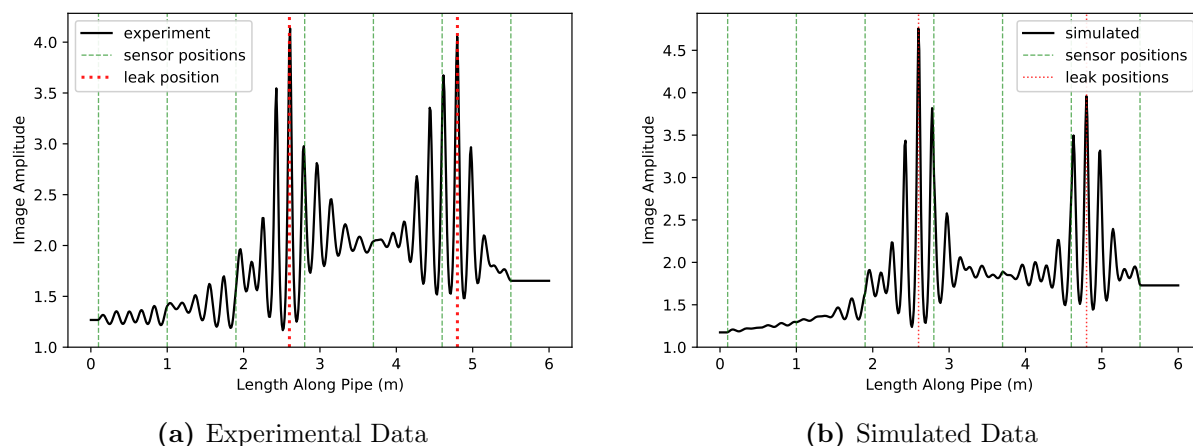**(a)** Experimental Data   **(b)** Simulated Data

Figure 6: Resultant image using the TR-MUSIC algorithm to successfully locate two noise sources on an experimental pipe rig (left). Data from a numerical simulation with matching parameters is shown for comparison (right). A frequency range of 450 Hz to 650 Hz is used for the analysis.

Two peaks in amplitude can be seen, which align with the simulated leak positions, showing that the algorithm has successfully resolved these two noise sources separately on a real water-filled pipe. The high-frequency sidelobes in the image are due to the use of frequencies which are above the sensor spacing (around 110 Hz for this setup). The exclusion of the lower frequencies is due to the poor response of the accelerometers below ~ 450 Hz. This was caused both by the pipe acting as a filter for those lower frequencies (also much higher frequencies), as well as resonances around 200 Hz. Although this effect obscures the peaks, the trend can still be seen.

As noted, the amplitude of these images is much smaller than the simulated examples in Section 4. The predominant reason for this is the effect of reflections, causing a misalignment with respect to the ideal response of the system being used. As shown in Fig. 5, the drop in peak amplitude is an expected effect of the reflections in a finite pipe. The simulated data (Fig. 6b) provides confidence in this, since a similar amplitude is achieved, as well as a similar overall shape of the image. In practice, this algorithm is designed to be used to find leaks on mains pipelines, which will stretch over kilometres rather than a few metres, so the effect of reflections

should become negligible. On the other hand, there will still be discontinuities in pipes such as joins and bends, which may still have an effect on the outcome of this procedure.

6. Conclusion

In the quest for improved leak detection capabilities, the full utilisation of modern sensing equipment is necessary. This paper has shown that the wealth of work done on array processing techniques, already utilised in many other domains, is applicable and very useful to the problem of leak detection in water pipelines, in particular the location of leaks. Subspace-based methods are key when considering the multiple leaks that will be incident on an array of sensors, of which the MUSIC algorithm was chosen for the present research. Numerical simulations show that this is an effective approach, with varying numbers of sensors and with some additional noise present. Not shown here, the method is also resilient to non-uniform sensor spacing, subject to the wavelength limitations and aliasing effects discussed in Section 4. Results from a preliminary experimental setup give some validation to this.

However, care must be taken when choosing the parameters - especially the frequency ranges used in the processing. This will depend on the length of the system under consideration, the number and spacing of the sensors being used, as well as the type of sensor used. All these aspects, as well as the effect of noise, require a more in-depth and systematically quantified analysis, which is a key aim of future research. Nevertheless, what is presented here gives a starting point for how a distributed sensing system for the purposes of leak location might look. The method outlined here assumes point sensors, and so is suitable for accelerometers and hydrophones already widely used by industry, as well as a rod method of leak location, being developed as part of the larger project that this work is part of.

References

[1] Gupta A and Kulat K D 2018 "A Selective Literature Review on Leak Management Techniques for Water Distribution System" *Water Resources Management* **32**

[2] Fuchs H V and Riehle R 1991 "Ten years of experience with leak detection by acoustic signal analysis" *Applied Acoustics* **33**

[3] Chiariotti P, Martarelli M and Castellini P 2019 "Acoustic beamforming for noise source localization – Reviews, methodology and applications" *Mechanical Systems and Signal Processing* **120**

[4] Schmidt R O 1986 "Multiple emitter location and signal parameter estimation." *IEEE Transactions on Antennas and Propagation* **AP-34** 276–280

[5] Prada C and Thomas J L 2003 "Experimental subwavelength localization of scatterers by decomposition of the time reversal operator interpreted as a covariance matrix" *The Journal of the Acoustical Society of America* **114** 235–243

[6] Lev-Ari H and Devancy A J 2000 "The time-reversal technique re-interpreted: Subspace-based signal processing for multi-static target location" *Proceedings of the IEEE Sensor Array and Multichannel Signal Processing Workshop* vol 2000-January (IEEE Computer Society) pp 509–513

[7] Fan C, Pan M, Luo F and Drinkwater B 2014 "Multi-frequency time-reversal-based imaging for ultrasonic nondestructive evaluation using full matrix capture" *IEEE Transactions on Ultrasonics, Ferroelectrics, and Frequency Control* **61**

[8] Muggleton J M, Brennan M J and Pinnington R J 2003 "Wavenumber prediction of waves in buried pipes for water leak detection" *Journal of Sound and Vibration* **249**

[9] Fuller C R and Fahy F J 1982 "Characteristics of wave propagation and energy distributions in cylindrical elastic shells filled with fluid" *Journal of Sound and Vibration* **81** 501–518

[10] Fuller C R 1983 "The input mobility of an infinite circular cylindrical elastic shell filled with fluid" *Journal of Sound and Vibration* **87** 409–427

[11] Pinnington R J and Briscoe A R 1994 "Externally applied sensor for axisymmetric waves in a fluid filled pipe" *Journal of Sound and Vibration* **173**